Micromechanical modelling of stress-induced phase transition in shape memory alloys

H. Petryk and S. Stupkiewicz
Institute of Fundamental Technological Research
Polish Academy of Sciences
Swietokrzyska 21, 00–049 Warsaw, Poland
e–mail: hpetryk@ippt.gov.pl, sstupkie@ippt.gov.pl

Abstract

A micro-mechanical model of stress-induced martensitic transformation in shape memory alloys is presented. A laminated microstructure of austenite and martensite phases is assumed along with a time-independent thermodynamic criterion for phase transformation. In numerical examples, the pseudoelastic behaviour of single crystals of CuZnAl and CuAlNi shape memory alloys is investigated. Several aspects are examined, including the effects of the loading direction, external constraints, detwinning, and instability of macroscopically uniform transformation.

1 Introduction

Shape memory alloys at a temperature high enough to ensure stability of the austenitic phase at zero stress, upon loading undergo stress-induced martensitic transformation. As commonly observed in experiments, the transformation proceeds by the formation and growth of martensitic plates within the austenite matrix. Upon unloading, the martensite is transformed back to austenite, which corresponds to pseudoelastic (or superelastic) behaviour of the material with a characteristic hysteresis loop on the stress-strain diagram, cf. e.g., [6].

In this paper, a micromechanical model is presented which provides a link between the structure and mechanical properties of shape memory materials at different scales of observation. One of the main objectives of micromechanics is to predict and explain the macroscopic behaviour in terms of the material microstructure and properties at a micro-scale where physical mechanisms of deformation are better recognized. It is natural to apply such approach to shape memory alloys in which the basic microstructural changes are related to crystal lattice rearrangements. The transition from transformations of the atomic structure to the behavior of a polycrystalline specimen is, however,

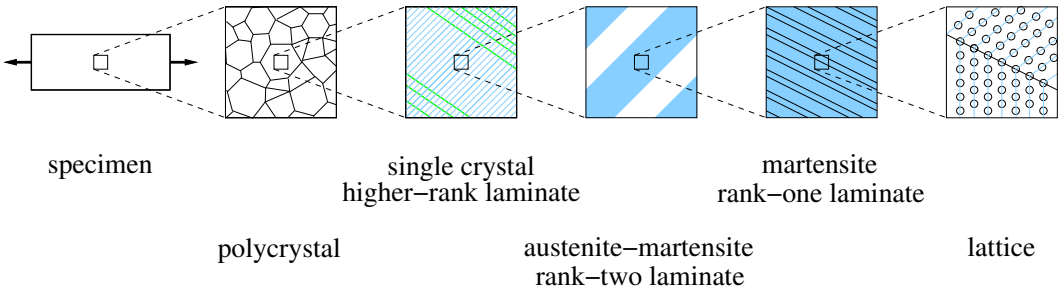

Figure 1: An example of a multi-scale modeling scheme.

not straightforward and requires consideration of intermediate levels. This leads to hierarchical, multi-scale micromechanical modeling that involves sequential transition between more than two different spatial (and also temporal) scales, Fig. 1.

A representative volume element of a polycrystalline material is used to describe overall properties of the material at the highest level. The transition to a still larger scale of a specimen can generally be accompanied by temperature nonuniformity and instability phenomena influenced by the specimen shape, dimensions and boundary conditions. Experiments show (e.g. [12, 18]) that the phase transformation process in polycrystalline specimens can proceed nonuniformly by propagation of transformation zones. In consequence, mechanical characteristics of the specimen can significantly differ from those of the material. The respective transition is not discussed in this paper being restricted to the modeling of the material itself.

The overall isothermal response of a polycrystalline aggregate can be simulated by using one of the known averaging methods. Several crystal-to-polycrystal transition schemes, not restricted to uniaxial models, have been applied to shape memory alloys, e.g. a self-consistent model [7], a layered model for textured polycrystals [14], a uniform strain model, and finite element discretization [19], to mention just a few examples. It is beyond the scope of this paper to discuss polycrystal models in more detail. For the present work it is only essential that effective methods exist for simulating a macroscopic response of a polycrystalline material starting from a model of a single crystal behavior.

This paper deals with the micromechanical modeling of a *single* crystal of a shape memory alloy undergoing stress-induced martensitic transformation at a given temperature. The analysis is restricted here to the multi-scale transition between the last three (or sometimes four) levels indicated in Fig. 1, starting from the crystallographic lattice transformations. The main assumption is that of a *laminated microstructure* within the crystal when the martensitic transformation is stress-induced; a similar concept has appeared earlier, e.g. in [10]. This assumption is motivated by the existing experimental evidence and simplifies considerably the description of mechanical interactions between the phases. The basic step of the analysis reduces to the micro-macro transition for a rank-one laminate, described in detail in [16], with due account for moving interfaces and differences in elastic anisotropy of the constituents. In this paper, some novel applications of the model developed by the authors in [16] are presented.

2 Micro-macro transition for evolving microstructures

2.1 Preliminaries

For simplicity, the considerations below are limited to the small deformation theory, although extensions to finite deformations are possible, cf. [8]. The macroscopic strain and stress in a volume V, distinguished from a local strain $\boldsymbol{\varepsilon}$ and stress $\boldsymbol{\sigma}$ by a superimposed bar, are given by the standard formulas

$$\bar{\boldsymbol{\varepsilon}} = \langle \boldsymbol{\varepsilon} \rangle \,, \qquad \bar{\boldsymbol{\sigma}} = \langle \boldsymbol{\sigma} \rangle \,, \qquad \langle \cdot \rangle \equiv \frac{1}{V} \int (\cdot)\, dV \,. \tag{1}$$

Analogously, $\bar{\phi} = \langle \phi \rangle$ is the macroscopic counterpart to the local Helmholtz free energy per unit volume, assuming temperature uniformity and no interface energy.

Sudden formation of a thin transformed layer within V corresponds to small changes in $\bar{\boldsymbol{\varepsilon}}$ and/or $\bar{\boldsymbol{\sigma}}$ accompanied by a substantial jump $\Delta\boldsymbol{\varepsilon}$ in *local* strain, and possibly also by a jump $\Delta\boldsymbol{\sigma}$ in local stress. When the process of phase transformation is smoothed out in time then small changes in $\bar{\boldsymbol{\varepsilon}}$ and $\bar{\boldsymbol{\sigma}}$, divided by a small time increment, are interpreted as *forward* rates, $\dot{\bar{\boldsymbol{\varepsilon}}}$ and $\dot{\bar{\boldsymbol{\sigma}}}$. Similarly, the transformed layer thickness is represented by its forward rate $\dot{s} \geq 0$ interpreted as the speed of a *regularized* transformation front. The local jumps $\Delta(\cdot) = (\cdot)^- - (\cdot)^+$ from the parent $(+)$ to product $(-)$ phases do not admit such a rate representation. Moreover, their distribution within an internally laminated plate is not smooth. Due to the existing irregularities, $\dot{\bar{\boldsymbol{\varepsilon}}}$ and $\dot{\bar{\boldsymbol{\sigma}}}$ are to be calculated by applying the transport theorem in an *extended* form [8], which yields

$$\dot{\bar{\boldsymbol{\varepsilon}}} = \langle \dot{\boldsymbol{\varepsilon}} \rangle + \frac{1}{V} \int_S \Delta\boldsymbol{\varepsilon}\, \dot{s}\; dS \,, \qquad \dot{\bar{\boldsymbol{\sigma}}} = \langle \dot{\boldsymbol{\sigma}} \rangle + \frac{1}{V} \int_S \Delta\boldsymbol{\sigma}\, \dot{s}\; dS \,. \tag{2}$$

Here, S denotes the set of all interfaces, and the prefix Δ denotes the forward jump with respect to *time* in a local variable on S, averaged over the layer thickness. Note that at an initial instant of phase transformation, spatial jumps are not yet present.

The continuity of displacements and equilibrium of stresses, assumed throughout the paper, imply

$$\Delta\boldsymbol{\varepsilon} = \tfrac{1}{2}(\mathbf{c} \otimes \mathbf{n} + \mathbf{n} \otimes \mathbf{c}) \,, \qquad \Delta\boldsymbol{\sigma}\, \mathbf{n} = \mathbf{0} \,, \tag{3}$$

where $\otimes$ denotes the tensor product, $\mathbf{n}$ is a unit normal to S and $\mathbf{c}$ is a vector such that $\dot{s}\mathbf{c}$ is the velocity jump across S. The local *thermodynamic driving force*, per unit area of the phase transformation front, has the familiar form

$$f = \boldsymbol{\sigma} \cdot \Delta\boldsymbol{\varepsilon} - \Delta\phi \,, \tag{4}$$

where the stress $\boldsymbol{\sigma}$ can be taken from any side of the front. Accordingly, the intrinsic dissipation rate due to the transformation is expressed by

$$\dot{\bar{\mathcal{D}}}^{\mathrm{t}} = \int_S \dot{\mathcal{D}}^{\mathrm{t}}\, dS \,, \qquad \dot{\mathcal{D}}^{\mathrm{t}} = f\, \dot{s} \geq 0 \,. \tag{5}$$

2.2 Basic microstructure

In accord with experimental observations, the stress-induced martensitic transformation in a single crystal of a shape memory alloy proceeds by the formation of parallel martensitic plates within an austenite matrix. Typically, a martensite plate can either involve only one crystallographic variant of martensite (usually with internal stacking faults) or be a fine mixture of two twin-related martensite variants. The corresponding microstructure is thus a rank-one laminate in the former case and a rank-two laminate in the later case.

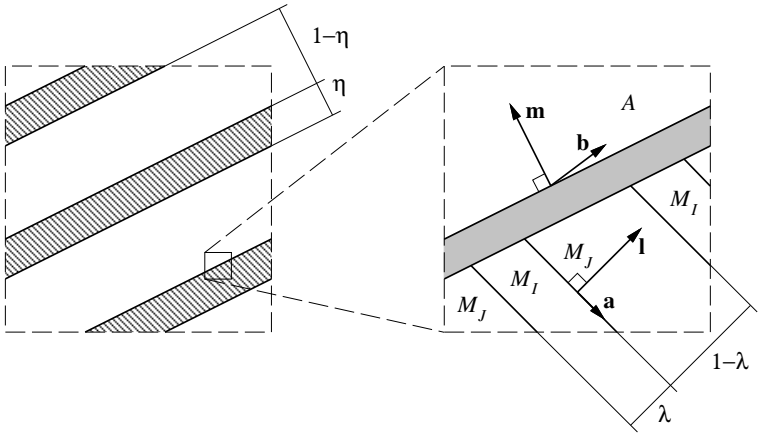

Figure 2: A schematic view of a periodic microstructure formed by internally twinned martensite plates within austenite matrix (A – austenite, M_I, M_J – martensite variants).

A single crystal of austenite may transform to several variants of martensite, indexed by I, with known transformation strain $\boldsymbol{\varepsilon}^{\mathrm{t}}_I$. Following [16], consider the microstructure associated with the formation of internally twinned martensite plates as shown in Fig. 2. The microstructural parameters can be determined, in the first approximation, from the crystallographic theory of martensitic transformation [20, 1], which can be adopted in the geometrically linear framework for small strains [2]. In this theory, compatibility between the *homogenized* phases is assumed to hold at zero stress. In the small strain format, this leads to the twinning equation

$$\boldsymbol{\varepsilon}^{\mathrm{t}}_I - \boldsymbol{\varepsilon}^{\mathrm{t}}_J = \tfrac{1}{2}(\mathbf{a}\otimes\mathbf{l} + \mathbf{l}\otimes\mathbf{a}) \tag{6}$$

with the unit vector $\mathbf{l}$ normal to the twin interface and a non-zero vector $\mathbf{a}$ as the unknowns, and the habit plane equation

$$\boldsymbol{\varepsilon}^{\mathrm{t}} = \tfrac{1}{2}(\mathbf{b}\otimes\mathbf{m} + \mathbf{m}\otimes\mathbf{b}) \tag{7}$$

with the unknowns $\mathbf{m}$ and $\mathbf{b}$ denoting, respectively, the unit vector normal to the austenite-martensite interface and a non-zero vector (shape strain). The *effective* transformation strain $\boldsymbol{\varepsilon}^{\mathrm{t}}$ in an internally twinned martensitic plate reads

$$\boldsymbol{\varepsilon}^{\mathrm{t}} = \lambda\boldsymbol{\varepsilon}^{\mathrm{t}}_I + (1-\lambda)\boldsymbol{\varepsilon}^{\mathrm{t}}_J \tag{8}$$

where λ denotes the (unknown) volume fraction of variant I in the plate. In turn, for an untwinned plate of martensite variant I with internal faults, where equation (6) does not apply, we have

$$\boldsymbol{\varepsilon}^{\mathrm{t}} = \boldsymbol{\varepsilon}^{\mathrm{t}}_I + k_{\mathrm{sf}} \frac{1}{2}(\mathbf{s}_I \otimes \mathbf{n}_I + \mathbf{n}_I \otimes \mathbf{s}_I) \tag{9}$$

where k_{sf} is the (unknown) magnitude of shear due to stacking faults, and $\mathbf{n}_I$ and $\mathbf{s}_I$ are known unit vectors normal to the shear plane and parallel to the shear direction, respectively.

By solving the above algebraic equations with respect to the unknowns, we obtain geometric characteristics of N distinct martensitic plates, indexed by $\alpha = 1, \ldots, N$. Subsequently, depending on the loading program, the preferred martensitic plates are selected by applying the transformation criterion, to be discussed in subsection 2.4. However, if detwinning within the twinned martensite plates *during* stress-induced transformation is accounted for then the twin fraction λ is not constant and transformation strain compatibility (7) no longer holds at zero stress. Consequences of this are indicated in subsection (3.2) and examined in more detail in [17].

Mechanical properties of each constituent at the micro-level are defined by the free energy functions for austenite (ϕ_{a}) and for I-th martensite variant (ϕ_I), assumed in the form

$$\phi_{\mathrm{a}} = \phi_0 + \tfrac{1}{2}\boldsymbol{\varepsilon} \cdot \mathbf{L}_{\mathrm{a}}\boldsymbol{\varepsilon}, \quad \phi_I = \phi_0 + \Delta^{\mathrm{am}}\phi_0 + \tfrac{1}{2}(\boldsymbol{\varepsilon} - \boldsymbol{\varepsilon}^{\mathrm{t}}_I) \cdot \mathbf{L}_I(\boldsymbol{\varepsilon} - \boldsymbol{\varepsilon}^{\mathrm{t}}_I)\,, \tag{10}$$

where ϕ_0 is the Helmholtz free energy density for austenite at zero stress at a given temperature, $\Delta^{\mathrm{am}}\phi_0$ is the temperature-dependent free energy jump due to martensitic transformation, taken at zero stress, while the quadratic terms represent the elastic energy due to non-zero local stresses in the phases.

2.3 Constitutive micro-macro transition for laminates

Laminated microstructures in shape memory alloys are particularly convenient from the point of view of micromechanical modelling since the micro-macro relationships can be derived analytically for these microstructures. The complete set of equations for two-phase rank-one laminates at small deformation can be found in [16]; for higher-rank laminates of separable scales the equations can be used sequentially. The derived expression for the bulk contribution to the overall Helmholtz free energy per unit representative volume of the austenite/martensite laminate as shown in Fig. 2 is

$$\bar{\phi} = \phi_0 + \eta\Delta^{\mathrm{am}}\phi_0 + \tfrac{1}{2}\bar{\boldsymbol{\sigma}} \cdot \tilde{\mathbf{M}}\bar{\boldsymbol{\sigma}} + \tfrac{1}{2}\eta(1-\eta)\boldsymbol{\varepsilon}^{\mathrm{t}} \cdot \mathbf{Q}\boldsymbol{\varepsilon}^{\mathrm{t}}\,, \tag{11}$$

where η is the total volume fraction of martensite and $\tilde{\mathbf{M}}$ is the effective elastic compliance tensor for the laminate. Interfacial energy effects are disregarded here. Under the assumption (7) of an invariant habit plane at zero stress, the product $\boldsymbol{\varepsilon}^{\mathrm{t}} \cdot \mathbf{Q}\boldsymbol{\varepsilon}^{\mathrm{t}}$ in (11) vanishes. In this case, the related thermodynamic driving force (4) corresponding to increasing η has been transformed to

$$f = -\partial\bar{\phi}/\partial\eta = \bar{\boldsymbol{\sigma}} \cdot \bar{\boldsymbol{\varepsilon}}^{\mathrm{t}} - \tfrac{1}{2}\bar{\boldsymbol{\sigma}} \cdot \mathbf{B}^T_{\mathrm{a}}(\mathbf{M}_{\mathrm{a}} - \mathbf{M}_{\mathrm{m}})\mathbf{B}_{\mathrm{m}}\bar{\boldsymbol{\sigma}} - \Delta^{\mathrm{am}}\phi_0\,, \tag{12}$$

with the first right-hand side term known as the Schmid factor and the second term, quadratic in $\boldsymbol{\sigma}$, being proportional to the difference between the elastic compliance tensor $\mathbf{M}_\mathrm{a}$ for austenite and the effective one $\mathbf{M}_\mathrm{m}$ for a martensite plate. Analytic expressions for $\mathbf{Q}, \tilde{\mathbf{M}}, \mathbf{M}_\mathrm{m}, \mathbf{B}_\mathrm{a}, \mathbf{B}_\mathrm{m}$ and further details are available in [16].

The averaged rates of stress and strain in a rank-one laminate are related by

$$\langle\dot{\boldsymbol{\sigma}}\rangle = \tilde{\mathbf{L}}\langle\dot{\boldsymbol{\varepsilon}}\rangle\,, \qquad \langle\dot{\boldsymbol{\varepsilon}}\rangle = \tilde{\mathbf{M}}\langle\dot{\boldsymbol{\sigma}}\rangle\,, \qquad \tilde{\mathbf{M}} = \tilde{\mathbf{L}}^{-1}\,. \tag{13}$$

provided no transformation occurs *inside* the layers.

Evolution of the layered microstructure can most simply be described when the transformation proceeds only between a fixed ordered pair of (+) and (−) phases treated as homogeneous. Then, equations (2) reduce to

$$\dot{\bar{\boldsymbol{\varepsilon}}} = \langle\dot{\boldsymbol{\varepsilon}}\rangle + \dot{\eta}^{-}\Delta\boldsymbol{\varepsilon}\,, \qquad \dot{\bar{\boldsymbol{\sigma}}} = \langle\dot{\boldsymbol{\sigma}}\rangle + \dot{\eta}^{-}\Delta\boldsymbol{\sigma}\,, \tag{14}$$

where η^{-} is the volume fraction of the product phase, and the jumps $\Delta\boldsymbol{\varepsilon}$ and $\Delta\boldsymbol{\sigma}$ are determined locally by solving (3) on moving interfaces. From (14) and (13) the plasticity-like macroscopic constitutive rate equations are obtained for a specified (+) → (−) transformation:

$$\dot{\bar{\boldsymbol{\varepsilon}}} = \tilde{\mathbf{M}}\dot{\bar{\boldsymbol{\sigma}}} + \dot{\eta}^{-}\boldsymbol{\mu}\,, \qquad \dot{\bar{\boldsymbol{\sigma}}} = \tilde{\mathbf{L}}\dot{\bar{\boldsymbol{\varepsilon}}} - \dot{\eta}^{-}\boldsymbol{\lambda}\,, \tag{15}$$

where

$$\boldsymbol{\lambda} = \tilde{\mathbf{L}}\Delta\boldsymbol{\varepsilon} - \Delta\boldsymbol{\sigma} = \tilde{\mathbf{L}}\boldsymbol{\mu}\,. \tag{16}$$

Equations (15) with (16) are valid for a rank-one laminated microstructure independently of the adopted criterion of phase transformation.

2.4 Criterion of phase transformation

The value of $\dot{\eta}^{-}$ is to be determined from a criterion of phase transition. Neglecting time-dependence effects, the local criterion for martensitic phase transformation is assumed in the form (cf. [9])

$$f - f_\mathrm{c} \le 0\,, \qquad (f - f_\mathrm{c})\dot{s} = 0\,, \qquad f_\mathrm{c} \ge 0\,, \tag{17}$$

where f is the thermodynamic driving force (4) and f_c is a threshold value related to the width of a hysteresis loop in a transformation cycle. In the following we take $f_\mathrm{c} = \mathrm{const}$, which is the simplest assumption.

A remarkable consequence [16] is that in the absence of dissipation due to reorientation of martensite variants, the intrinsic dissipation $\bar{\mathcal{D}}^\mathrm{t}$ due to any transformation in a volume V^t is

$$\bar{\mathcal{D}}^\mathrm{t} = V^\mathrm{t} f_c \tag{18}$$

separately for forward and reverse transformation. It follows that for a closed transformation cycle in a given volume V^t, the area of a hysteresis loop does not depend on the loading program (e.g. tension or compression, loading direction, etc.).

By using the criterion (17), for a given loading program the preferred martensite plate is selected for which the respective transformation condition $f - f_\mathrm{c} = 0$ is satisfied

first. This defines the parameters of the $(+) \to (-)$ transformation that is followed in subsequent calculations as long as another transformation is preferred by the criterion (17).

From (17) with $f_c = \text{const}$ after certain rearrangements the following *macroscopic* criterion for a specified $(+) \to (-)$ transformation is obtained [8, 16]

$$\begin{aligned} \dot{\eta}^- &= \frac{1}{g}\boldsymbol{\lambda} \cdot \dot{\bar{\boldsymbol{\varepsilon}}} > 0 \qquad && \text{if } \eta^- < 1 \text{ and } f = f_c \text{ and } \boldsymbol{\lambda} \cdot \dot{\bar{\boldsymbol{\varepsilon}}} > 0\,, \\ \dot{\eta}^- &= 0 && \text{otherwise}\,. \end{aligned} \tag{19}$$

In consequence, an increment in the volume fraction η^- of the product phase is explicitly related to an increment in the overall strain $\bar{\boldsymbol{\varepsilon}}$, with the help of two quantities, $\boldsymbol{\lambda}$ defined by (16) and g defined by

$$g = \Delta\boldsymbol{\varepsilon} \cdot \tilde{\mathbf{L}} \Delta\boldsymbol{\varepsilon}\,, \tag{20}$$

with $g > 0$ if the laminate is *elastically* stable.

Substitution of (19) into (15) yields

$$\dot{\boldsymbol{\sigma}} = \tilde{\mathbf{L}}^{\mathrm{t}} \dot{\bar{\boldsymbol{\varepsilon}}}\,, \qquad \tilde{\mathbf{L}}^{\mathrm{t}} = \tilde{\mathbf{L}} - \frac{1}{g}\boldsymbol{\lambda} \otimes \boldsymbol{\lambda} \qquad \text{if } \dot{\eta}^- > 0 \text{ and } f_c = \text{const}\,, \tag{21}$$

where $\tilde{\mathbf{L}}^{\mathrm{t}}$ is the overall tangent moduli tensor for a rank-one laminate undergoing martensitic phase transformation. In multiscale modeling, it can be used as a local tangent moduli tensor of a higher-level laminate.

The constitutive framework in the rate form shown above is useful in establishing qualitative properties of the material behavior. Step-by-step calculations can be performed with the help of analytic expressions for the jumps $\Delta\boldsymbol{\varepsilon}$ and $\Delta\boldsymbol{\sigma}$ on interfaces and the effective stiffness and compliance tensors $\tilde{\mathbf{L}}$ and $\tilde{\mathbf{M}}$, given in the matrix form in [16] for arbitrary anisotropic linear elastic materials with eigenstrains. The task is simplified for the transformation between a fixed pair of $(+)$ and $(-)$ phases without elastic unloading or reverse transition since then the value of η^- corresponding to the current $\bar{\boldsymbol{\varepsilon}}$ can be found directly from the algebraic condition $f = f_c$. In general, the volume fractions of the parent and product phases are also dependent on the history of $\bar{\boldsymbol{\varepsilon}}$, which is associated with the appearance of hysteresis loops.

3 Examples

3.1 Untwinned martensite in CuZnAl

As the first example of application of the model outlined above, consider the stress-induced cubic-to-monoclinic transformation in a CuZnAl alloy. In this transformation the cubic austenite of DO_3 structure transforms to the monoclinic martensite of 18R structure (also called 6M structure). The martensite forms untwinned plates in which compatibility at the austenite-martensite interface is provided by random stacking faults (sequence faults) on the basal (101) planes [4, 15].

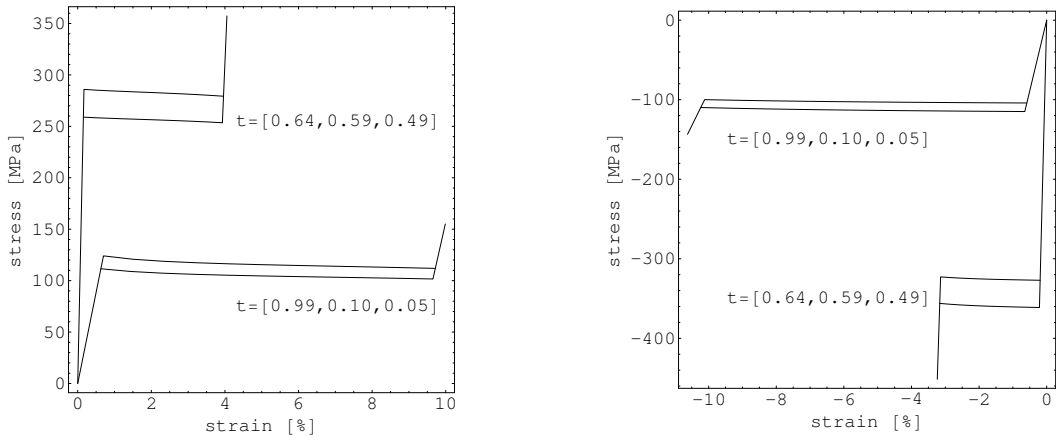

(a) (b)

Figure 3: Overall stress-strain diagrams in uniaxial tension (a) and compression (b) of CuZnAl crystal for two loading directions

The material parameters, i.e. the crystallographic lattice parameters and the elastic constants of single-crystalline austenite and martensite, are taken from the available literature. Parameters of $N = 24$ symmetry-related martensitic plates, i.e. the habit plane normal $\mathbf{m}$, shape strain vector $\mathbf{b}$ and shear magnitude due to stacking faults $k_{\rm sf}$ are calcualted from (7) and (9). Numerical values of all these parameters along with the relevant references are given in [15]. The actually preferred plate is selected by using the transformation criterion (17).

Figure 3 shows the isothermal stress-strain diagrams corresponding to loading and unloading under uniaxial tension and compression (with axial strain control) for two loading directions specified by vector $\mathbf{t}$ relative to the cubic basis of austenite as indicated in the figure. The calculations have been performed for the value of chemical energy $\Delta^{\rm am}\phi_0 = 10\,[{\rm MJ/m^3}]$ and the critical thermodynamic driving force $f_c = 0.5\,[{\rm MJ/m^3}]$. The overall stress-strain diagrams correspond to the formation of a single family of martensite plates in austenite under loading in two crystallographically distinct directions, and to the reverse transformation upon unloading. A strong effect of the crystal anisotropy is visible as the influence of the loading direction on the material response. However, the area of different hysteresis loops is invariant, in accord with the formula (18).

3.2 Twinned martensite in CuAlNi

Consider now the case of internally twinned martensite plates. As an example we take isothermal stress-induced cubic (β_1) to orthorhombic (γ_1') transformation in a single crystal of a CuAlNi shape memory alloy. There are 6 crystallographic variants of martensite which, according to the theory outlined above, can form $N = 96$ distinct martensitic plates.

Three parameters of the transformation strain, three elastic constants for austenite and

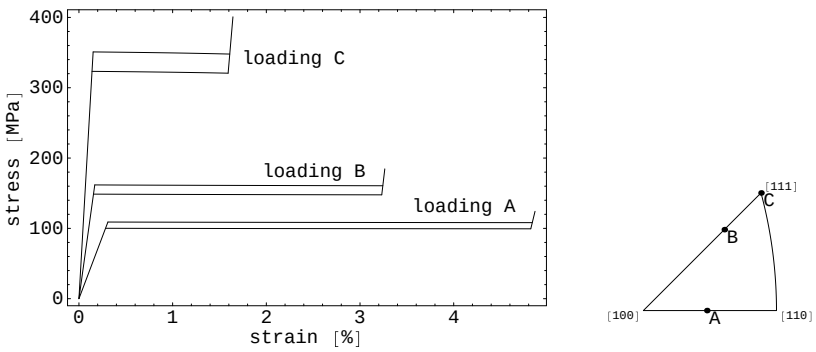

Figure 4: Overall stress-strain plots in uniaxial tension of CuAlNi single crystal undergoing $\beta_1 \to \gamma_1'$ transformation for three loading directions [16].

nine for martensite are taken from the literature. The temperature-dependent parameter $\Delta^{\rm am}\phi_0$ and constant $f_{\rm c}$ in (17) have been selected to fit the uniaxial stress-strain data for tensile specimen A1T1 in [13]. The numerical values of all these experiment-based parameters and the respective references are provided in [16]; no other material parameters are required to perform the calculations.

Sample results of small-strain calculations for an isothermal uniaxial tension test (under axial strain control) are shown in Fig. 4. Similar graphs were recently obtained in [3] by using another model. The overall stress-strain diagrams correspond to the formation of a single family (selected by using the transformation criterion (17)) of internally twinned martensitic plates in austenite under tension in three crystallographically distinct directions, and to the reverse transformation upon unloading. It must be noted, however, that the assumption of $\beta_1 \to \gamma_1'$ transformation may not correspond to reality since other transformation types are also possible in CuAlNi, cf. [5].

The diagrams presented in Figs. 4 and 3 are similar in character. Due to the difference in elastic properties of the phases, the internal stresses vary as the transformation proceeds with an increasing volume fraction of martensite, although the overall stress is almost constant (actually slightly decreasing in absolute value).

The results are significantly different if detwinning, i.e. martensite variant rearrangement by propagation of twinning planes, is taken into account, which was ruled out naturally in untwinned martensite and artificially when calculating the diagrams in Fig. 4. As discussed in [11, 17], detwinning can induce a drop of the overall uniaxial tensile stress even to zero as austenite diappears.

The detwinning effect can be not so strong, but still significant, in the presence of kinematic constraints. In the examples discussed above, a crystal could deform freely under uniaxial loading. This is a highly idealized situation for a grain in a polycrystal, but also for a specimen whose deformation is constrained by grips. The effect of such constraints can be illustrated by the example of a tensile specimen with the superimposed kinematic constraint $\varepsilon_{12} = 0$ (so that $\sigma_{12} \neq 0$) as indicated in Fig. 5; the directions $\mathbf{t}$ and $\mathbf{s}$ are given relative to the cubic basis of austenite. The resulting stress-strain curve in loading is shown in Fig. 5 by a broken line in the case of prohibited detwinning, and by a

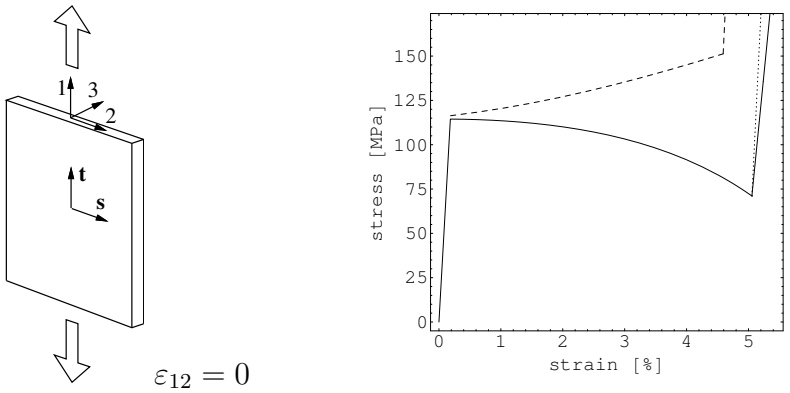

Figure 5: Constrained tension of CuAlNi single crystal undergoing $\beta_1 \rightarrow \gamma_1'$ transformation for $\mathbf{t} = [0.925, 0.380, 0.]$ and $\mathbf{s} = [-0.380, 0.925, 0.]$. A solid line corresponds to free detwinning and a dashed line to a fixed twin fraction λ.

solid line in the case of fully mobile twinning planes within martensite plates. Detwinning is *not* completed when austenite diappears at the lowest stress point and is continued with increasing stress. The apparent stiffness of martensite thus differs from the purely elastic behaviour of martensite indicated by a dotted line; cf. [17] for a more detailed discussion.

It must be emphasized that the material response has been calculated under the assumption of a *uniformly* laminated microstructure. However, due to the instability related to the softening behaviour, the transformation pattern of a specimen may be strongly non-uniform macroscopically. This can happen also in the absence of detwinning and irrespective of external boundary constraints, which is examined in the next subsection.

3.3 Instability of macroscopically uniform transformation

Consider the so-called *acoustic tensor* $\mathbf{A} = \mathbf{n}\tilde{\mathbf{L}}^{\mathrm{t}}\mathbf{n}$, defined by contracting the tangent stiffness tensor $\tilde{\mathbf{L}}^{\mathrm{t}}$ from both sides with some unit vector $\mathbf{n}$. A detailed study of the form of $\tilde{\mathbf{L}}^{\mathrm{t}}$ specified by (21), (16) and (20) shows that the lowest eigenvalue of $\mathbf{A}$ for some $\mathbf{n}$ is, as a rule, *negative* (or zero in particular cases). Consequently, the macroscopically uniform transformation process, which at a micro-scale produces a fine rank-one laminate, may be regarded as intrinsically unstable. Even if this conclusion may be mitigated by realizing that an infinitely fine laminate is only an idealization, the tendency to build up more complex patterns, e.g. higher-rank laminated microstructures, may be expected. The idea of relating the formation of complex martensitic microstructures to an intrinsic instability of *macroscopically* uniform transformation is presented here only in outline; a more detailed exposition will be given elsewhere.

For example, in the tensile test simulation for loading A in Fig. 4 there exists a *bifurcation* of the layered transformation pattern, sketched (not to scale) in Fig. 6. The upper pattern (I) is that assumed earlier to be macroscopically uniform, i.e. to cover the volume fraction $\eta_0 = 1$ of the whole material. However, an alternative solution (II) exists in which the primary (internally twinned) martensitic plates first appear within a certain volume fraction $\eta_0 < 1$ only, while the remaining part of austenite undergoes

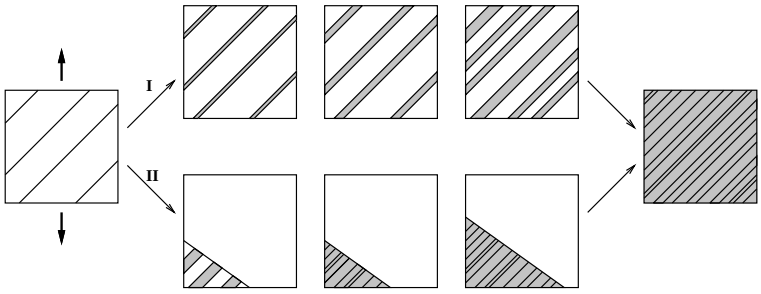

Figure 6: Bifurcation of the layered transformation pattern: the transformation can proceed quasi-uniformly (upper pattern I) or be completed first within some volume fraction of the material (lower pattern II).

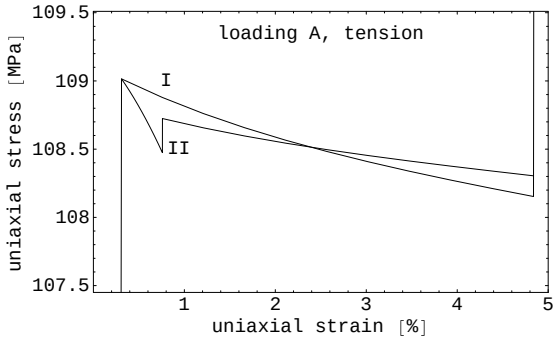

Figure 7: Overall stress-strain diagrams in uniaxial tension for two solutions corresponding to transformation patterns I and II in Fig. 6, with $\eta_0 = 0.1$ in case II.

unloading. These two regions are separated by parallel planes (only one such plane appears in schematic Fig. 6), forming thus a rank-three laminated microstructure. Across these separation planes, the kinematic and static compatibility conditions analogous to (3) can be satisfied after lower-level averaging. This is found to be the case if the separation planes are orthogonal to the vector $\mathbf{b}$ that appears in (7).

The corresponding macroscopic stress-strain diagrams are shown in Fig. 7. Compared to the macroscopically uniform pattern (I), the solution with $\eta_0 = 0.1$ is energetically preferable initially. When the transformation within the volume fraction η_0 is completed, a short period of fully elastic straining follows, accompanied by a sharp increase in stress. Next, after reaching the threshold value f_c by the corresponding thermodynamic driving force, the martensite region starts to grow through propagation of the separation planes. In this case, the final microstructure reached on both routes is the same, as indicated in Fig. 6, which need not be the rule.

Other examples as well as extensions to finite deformation and internal length scale effects are currently being investigated.

Acknowledgement This work has been supported by the State Committee for Scientific Research (KBN), Poland, Grant No. 4 T07A 032 26.

References

[1] J.M. Ball and R.D. James. Fine phase mixtures as minimizers of energy. *Arch. Ration. Mech. An.*, 100:13–50, 1987.

[2] K. Bhattacharya. Comparison of the geometrically nonlinear and linear theories of martensitic transformation. *Continuum Mech. Thermodyn.*, 5:205–242, 1993.

[3] P. Blanc and C. Lexcellent. Micromechanical modelling of CuAlNi shape memory alloy behaviour. *Mater. Sci. Eng.*, A378:465–469, 2004.

[4] K.F. Hane. Bulk and thin film microstructures in untwinned martensites. *J. Mech. Phys. Solids*, 47:1917–1939, 1999.

[5] V. Novák, P. Šittner, and J. Van Humbeeck. Martensitic transformations of Cu-Al-Ni single crystals in tension/compression. *J. Physique IV*, 11:191–196, 2001.

[6] K. Otsuka and C.M. Wayman, editors. *Shape Memory Materials*. Cambridge University Press, 1998.

[7] E. Patoor, A. Eberhardt, and M. Berveiller. Thermomechanical behaviour of shape memory alloys. *Arch. Mech.*, 40(5–6):775–794, 1988.

[8] H. Petryk. Macroscopic rate-variables in solids undergoing phase transformation. *J. Mech. Phys. Solids*, 46:873–894, 1998.

[9] J.R. Rice. Continuum mechanics and thermodynamics of plasticity in relation to microscale deformation mechanisms. In A.S. Argon, editor, *Constitutive Equations in Plasticity*, pages 23–79. MIT Press, Cambridge, Mass., 1975.

[10] A.L. Roytburd and J. Slutsker. Deformation of adaptive materials. Part I. Constrained deformation of polydomain crystals. *J. Mech. Phys. Solids*, 47:2299–2329, 1999.

[11] A.L. Roytburd and J. Slutsker. Deformatin of adaptive materials. Part III: Deformation of crystals with polytwin product phases. *J. Mech. Phys. Solids*, 49:1795–1822, 2001.

[12] J.A. Shaw and S. Kyriakides. Thermomechanical aspects of NiTi. *J. Mech. Phys. Solids*, 43:1243–1281, 1995.

[13] T.W. Shield. Orientation dependence of the pseudoelastic behavior of single crystals of Cu–Al–Ni in tension. *J. Mech. Phys. Solids*, 43:869–895, 1995.

[14] Y.C. Shu and K. Bhattacharya. The influence of texture on the shape-memory effect in polycrystals. *Acta Mater.*, 46(15):5457–5473, 1998.

[15] S. Stupkiewicz. The effect of stacking fault energy on the formation of stress-induced internally faulted martensite plates. *Eur. J. Mech. A/Solids*, 23(1):107–126, 2004.

[16] S. Stupkiewicz and H. Petryk. Modelling of laminated micro-structures in stress-induced martensitic transformation. *J. Mech. Phys. Solids*, 50:2303–2331, 2002.

[17] S. Stupkiewicz and H. Petryk. Micromechanical modelling of stress-induced martensitic transformation and detwinning in shape memory alloys. *Journal de Physique IV*, 115:141–149, 2004.

[18] Q.-P. Sun and Z.-Q. Li. Phase transformation in superelastic NiTi polycrystalline micro-tubes under tension and torsion—from localization to homogeneous deformation. *Int. J. Sol. Struct.*, 39:3797–3809, 2002.

[19] P. Thamburaja and L. Anand. Polycrystalline shape-memory materials: effect of crystallographic texture. *J. Mech. Phys. Solids*, 49:709–737, 2001.

[20] M.S. Wechsler, D.S. Lieberman, and T.A. Read. On the theory of the formation of martensite. *Trans. AIME J. Metals*, 197:1503–1515, 1953.